



Published in final edited form as:

Neuroimage. 2016 November 15; 142: 421–430. doi:10.1016/j.neuroimage.2016.07.001.

Biophysical modeling of high field diffusion MRI demonstrates micro-structural aberration in chronic mild stress rat brain

Ahmad Raza Khan^{#1}, Andrey Chuhutin^{#1}, Ove Wiborg², Christopher D Kroenke³, Jens R. Nyengaard⁴, Brian Hansen¹, and Sune Nørhøj Jespersen^{1,5}

¹Center of Functionally Integrative Neuroscience, Aarhus University Hospital, Aarhus, Denmark

²Translational Neuropsychiatry Unit, Aarhus University, Risskov, Denmark

³Advanced Imaging Research Center, Oregon Health & Science University, Portland, Oregon, United States.

⁴Stereology and Electron Microscopy Laboratory, Centre for Stochastic Geometry and Advanced Bioimaging, Aarhus University, Aarhus, Denmark

⁵Department of Physics and Astronomy, Aarhus University, Aarhus, Denmark

These authors contributed equally to this work.

Abstract

Depression is one of the leading causes of disability worldwide. Immense heterogeneity in symptoms of depression causes difficulty in diagnosis, and to date, there are no established biomarkers or imaging methods to examine depression. Unpredictable chronic mild stress (CMS) induced anhedonia is considered to be a realistic model of depression in studies of animal subjects. Stereological and neuronal tracing techniques have demonstrated persistent remodeling of microstructure in hippocampus, prefrontal cortex and amygdala of CMS brains. Recent developments in diffusion MRI (d-MRI) analyses, such as neurite density and diffusion kurtosis imaging (DKI), are able to capture microstructural changes and are considered to be robust tools in preclinical and clinical imaging. The present study utilized d-MRI analyzed with a neurite density model and the DKI framework to investigate microstructure in the hippocampus, prefrontal cortex, caudate putamen and amygdala regions of CMS rat brains by comparison to brains from normal controls. To validate findings of CMS induced microstructural alteration, histology was performed to determine neurite, nuclear and astrocyte density. d-MRI based neurite density and tensor-based mean kurtosis (MKT) were significantly higher, while mean diffusivity (MD), extracellular diffusivity (D_{eff}) and intra-neurite diffusivity (D_L) were significantly lower in the amygdala of CMS rat brains. D_{eff} was also significantly lower in the hippocampus and caudate putamen in stressed groups. Histological neurite density corroborated the d-MRI findings in the amygdala and reductions in nuclear and astrocyte density further buttressed the d-MRI results. The present study demonstrated that the d-MRI based neurite density and MKT can reveal specific microstructural

Corresponding Author: Sune N. Jespersen, sune@cfi.au.dk.

Publisher's Disclaimer: This is a PDF file of an unedited manuscript that has been accepted for publication. As a service to our customers we are providing this early version of the manuscript. The manuscript will undergo copyediting, typesetting, and review of the resulting proof before it is published in its final citable form. Please note that during the production process errors may be discovered which could affect the content, and all legal disclaimers that apply to the journal pertain.

changes in CMS rat brains and these parameters might have value in clinical diagnosis of depression and for evaluation of treatment efficacy.

Keywords

Chronic mild stress; diffusion; Neurite density; Kurtosis; Amygdala; Histology

INTRODUCTION

Chronic stress exposure is one of the leading causes in the development of psychopathologies, of which depression is the dominant cause of disability worldwide (Ferrari et al., 2013; Mathers et al., 2008). An immense heterogeneity of symptoms are observed in depression, where the diverse array of underlying distinct pathophysiology make accurate preclinical modeling of the disease extremely challenging (Egeland et al., 2015; Nestler et al., 2002; Wiborg, 2013). Therefore, despite the prevalence of depression and its considerable impact on health and disease, the understanding of its pathogenesis and pathophysiology is still in its infancy. To date, depression is neither diagnosed with objective tests nor any gross brain pathology, but instead diagnosis relies on reported symptoms being matched to symptoms listed in the Diagnostic and Statistical Manual of Mental Disorders V (American Psychiatric Association, 2013). Recently, it has been proposed that impairment of neuroplasticity and cellular resilience might be key in the pathophysiology of mood disorders, and might be caused by alteration in neurogenesis (Jayatissa et al., 2006), long-term potentiation (LTP), axonal sprouting (Krishnan and Nestler, 2008; Manji et al., 2000), synaptic and dendritic remodeling (Christoffel et al., 2011; Mitra et al., 2005; Vyas et al., 2002), inflammatory cytokines and/or neurotrophic factors and glutamate (Cohen et al., 2014; De Kloet et al., 2005; Egeland et al., 2015). More recently, clinical and preclinical studies have used stereology and neuronal tracing techniques in postmortem brain tissue to establish significant structural and morphological changes of neurons and glial cells in prefrontal cortex (pfc) (Radley et al., 2004; Radley et al., 2006; Rajkowska, 2000; Rajkowska et al., 1999), hippocampus (Hp) (Cohen et al., 2014; Stockmeier et al., 2004; Vyas et al., 2002), amygdala (Am) (Bourgin et al., 2015; Bowley et al., 2002; Boyle, 2013; Mitra et al., 2005; Vyas et al., 2002) and caudate putamen (Cp) (y Palacios et al., 2014). Stereology based cell counting, cellular morphometry and neuronal tracing techniques have high sensitivity, specificity, and can contribute significantly to the understanding of microstructural remodeling in connection to stress. When used pre-clinically in combination with clinically applicable imaging techniques these methods may improve interpretation of neuroimaging findings. However, neuronal tracing techniques and stereology cannot be used for routine disease diagnosis and treatment monitoring. In contrast, non-invasive neuroimaging methods are either not sensitive enough to capture subtle microstructural modification in normal appearing brain regions or not specific enough to support biological interpretations. However, the recent development of diffusion magnetic resonance imaging (d-MRI) based neurite density measurement (Jespersen et al., 2010; Jespersen et al., 2007) and diffusion kurtosis imaging (DKI) parameters (Hansen et al., 2013; Jensen et al., 2005) have shown promise in offering sufficient sensitivity and/or specificity to characterize microstructural changes.

Animals exposed to a set of different stressors for variable time span is implemented as an unpredictable CMS animal model of depression. This model mimics aspects of human depression and can serve as a useful tool for advancing the understanding of disease pathology, e.g. the biological mechanisms underlying region specific changes, and can potentially lay a foundation for the development of therapeutic intervention strategies (Jayatissa et al., 2006; Wiborg, 2013; Willner, 2005). Neuronal tracing techniques have revealed contrasting effects on Hp and Am, such as dendritic atrophy and hypertrophy respectively, after different stress paradigms (Cohen et al., 2014; Henckens et al., 2015; Vyas et al., 2002). Concomitant responses in multiple regions such as the Hp, Am, Pfc and Cp are important because they suggest that stress might alter entire networks in a way that is best understood by integrating stress effects across multiple brain regions (Cohen et al., 2014; Henckens et al., 2015; Vyas et al., 2002; y Palacios et al., 2014). A strength of MRI is its ability to characterize the entire brain. Recent MRI studies have reported changes in water diffusion properties consistent with cellular atrophy, dendritic remodeling and volume alterations in different regions of the chronic stress at brain (Anacker et al., 2015; Bourgin et al., 2015; Henckens et al., 2015; Vestergaard-Poulsen et al., 2011).

However, quantitative histological data were not available to corroborate the MRI findings in any of these studies, and only one employed biophysical modeling of microstructural features affecting d-MRI. Therefore, imaging biomarkers sensitive to plastic changes in CMS remain difficult to interpret specifically in terms of the underlying microstructure.

The objective of the present study was to use biophysically informed d-MRI to characterize microstructural changes due to unpredictable CMS in gray matter regions of the brain, particularly Pfc, Cp, Am and Hp (Figure 1), and to support our findings with quantitative histology. Ex-vivo d-MRI was performed on the left hemisphere of control and CMS rat brains and analyzed in terms of quantitative biophysical modeling as well as DKI. The same hemispheres were also used for immune histological staining of astrocyte cells and fluorescent staining with lipophilic dye (DiI) and nuclear stain (Hoechst) for neurite and nuclear components respectively. New image post-processing methods were applied to obtain quantitative estimates of the volume fractions of these components. The study highlights the sensitivity of the Am region of the brain towards unpredictable CMS exposure, and indicates a potential for the MR based neurite density, mean tensor kurtosis, D_{eff} and D_{\perp} to be used to detect microstructural modifications in normal appearing brain regions (Enzinger et al., 2015; Hori et al., 2012).

METHODS

Animals

Twenty four adult male wistar rats (Taconic, Denmark) were used in the present study. Prior to group allocation, rats were exposed to unpredictable mild stressors for 8 weeks, and were subsequently identified as anhedonic (N=8) or resilient (N=8) based on a sucrose consumption test as described elsewhere (Wiborg 2013). An unexposed, age matched group (N=8) served as control. After completion of the stress paradigm, control and stressed rats were exsanguinated during intra-aortic perfusion fixation with isotonic saline containing heparin (10 IU/mL) followed by 4% buffered paraformaldehyde (pH 7.4). Brains of control

and stressed rats were removed and immersion fixed in fresh paraformaldehyde solution until the MRI experiment. All animal handling and treatment procedures were performed in accordance with the national guidelines for animal research, and after permission from the Animal Experiments Inspectorate of the Danish ministry of Food, Agriculture and Fisheries, Denmark.

Imaging Protocol

MRI experiments were performed on the left hemisphere of each brain (N=24). Brains were washed in phosphate-buffered saline solution (PBS) for 48 hours prior to MRI data acquisition to remove paraformaldehyde and minimize associated T_2 -related signal attenuation. Each cerebral hemisphere was placed into a MRI compatible tube filled with a magnetic susceptibility-matching and thermo-stable fluid (Fluorinert FC-40,3M Zwijndrecht, Belgium). All MRI data acquisition was performed on a 9.4T Bruker Biospec preclinical MRI system (Bruker Biospin, Germany) using a 15 mm bore mounted quadrature volume coil and high-power gradients (BGA12S-HP, Bruker Biospin, Germany) capable of a maximum gradient strength of 660 mT/m. Data acquisition was performed at room temperature (21°C) and standard diffusion protocol was used with spin echo preparation with one shot per k-space line. The diffusion weighted images (total 168 images) for biophysical modeling were acquired with 12 fixed directions and 14 b-values (the shells of $b=0, 500, 1000, 1500, 2000, 2500, 3000, 3500, 4000, 4500, 5000, 6000, 7000, 8000$ s/mm², corresponding to a range of gradient strengths of 0-580 mT/m). Simulations based on a large data set from rat brain (Hansen and Jespersen, 2016) were used to ensure that an adequate number of sampling directions for neurite density estimation in gray matter was acquired (>10 with this number of shells and gradient capability). Images were acquired coronally with 250 μ m isotropic resolution with the following parameters: TR/TE =6500 ms/26 ms, δ 15/5 ms, field of view (FOV) 25.5 \times 12.5 mm and matrix size 102 \times 50. Corresponding high resolution T2 weighted image slices (62.5 μ m in plane resolution and 250 μ m slice thickness) were also acquired using a RARE (Rapid acquisition with relaxation enhancement) sequence (TR/TE = 3500/11 ms, averages = 16 and matrix size 408 \times 200). The data acquisition took about 20 h of scan time for each brain. Prior to data analysis, diffusion weighted and T2-weighted images, both were compared and manually inspected for quality and movement. This procedure revealed no movement or misalignment and consequently no need for image registration. This was verified during the ROI delineation procedure. Recent studies have shown the presence of Gibbs ringing in d-MRI data to severely impact parameter estimation and have demonstrated a number of strategies to suppress the artifact prior to analysis (Kellner et al., 2015; Perrone et al., 2015; Veraart et al., 2015). In the present study, Gaussian low pass filtering was employed for smoothing the data to reduce the Gibbs ringing artefacts, similar to previously published methods (Tabesh et al., 2011; Veraart et al., 2015).

Parameter estimation

All diffusion weighted images were fit to the biophysical d-MRI model in a voxel-wise manner using the nonlinear least squares Levenberg–Marquardt algorithm as implemented in Matlab (The Mathworks Inc, Natick, MA). The 18-parameter model is recounted in detail in (Jespersen et al., 2010; Jespersen et al., 2007). Briefly, it describes diffusion in terms of an

isotropic Gaussian diffusion component (extracellular space, glial cells, and cell bodies) together with a population of cylinders representing axons and dendrites (collectively referred to as neurites) and the associated neurite orientation distribution. Main model parameters are: S_0 is a normalization parameter, ν is neurite density, D_L is the intra-neurite parallel diffusivity, D_{eff} diffusivity in extra-neurite space, and the remaining parameters describe the neurite orientation distribution (coefficients of its spherical harmonics expansion of order 4). When reporting results for the neurite density parameter, voxels were only included in the analysis if the sum of the squared errors between real and the estimated signals (both normalized) was less than 0.1. This threshold corresponds roughly to allowing the fitted data points to deviate from the measurements by an amount corresponding to the noise level of our experiments. The only constraint enforced in the fitting was the positivity of the diffusivities. For a subset of 50 randomly chosen voxels, the fitting procedure was repeated 1000 times with randomized initial values in order to explore the existence of multiple minima and the robustness of the fitting procedure.

For diffusion kurtosis, a conventional non-linear least squares fitting procedure was performed on a subset of the diffusion data (Jensen and Helpert, 2010) with b-values 0, 500, 1000, 1500, 2000, 2500, 3000, 3500, 4000, 4500s/mm² and all 12 directions to estimate kurtosis parameters. The higher b-value diffusion data was not included in order to not exceed the validity range of diffusion kurtosis imaging (Jensen and Helpert, 2010; Jensen et al., 2005). The same quality of fit criteria described above was applied, in addition to two other constraints: 1) the apparent excess kurtosis must be positive along a large number of directions (Veraart et al., 2011); and 2) an upper (b-dependent) bound on

$K \left(K(\hat{n}) \leq \frac{3}{D(\hat{n})b_{max}} \right)$ ensuring the signal to be a monotonically decreasing function of the b-value along any experimentally acquired direction. Furthermore, the diffusion tensor eigenvalues were constrained to be nonnegative. No more than 10 percent of voxels were excluded in average per slice, and this was not significantly different across the three groups. Moreover, less than 0.5 % of voxels within each of the ROIs were excluded. Parameters considered were mean diffusivity (MD), fractional anisotropy (FA) (Basser, 1995, 1997), mean kurtosis (MK) (Jensen et al., 2005), and mean of the kurtosis tensor (MKT) (Hansen et al., 2013).

The study explored four different regions of the brain to identify microstructural alteration due to unpredictable CMS in rat brain. The regions of interest (ROIs), Pfc, Hp, Am and Cp were delineated on the corresponding high resolution T₂-weighted images in a blinded way with reference to a rat brain atlas (George and Charles, 1998) and applied to the parameter maps (Figure 1 and Figure 2). Limits for the Pfc, Hp, Am and Cp were delineated within the regions as defined by the earlier studies (Bourgin et al., 2015; Henckens et al., 2015; Kalisch et al., 2006). Prior to analysis the T₂ weighted anatomical images of brains were inspected visually. It was found that perfusion had failed in one brain in the control group and in the anhedonic group two brains had partial physical damage. These samples were excluded from the study.

Histology

After MRI scans, all the left brain hemispheres were rinsed with PBS and again immersed into the paraformaldehyde solution until sectioning. They were then embedded in 5% agar and 60 μm thick horizontal sections were cut on a Vibratome 3000 (Vibratome Co., St. Louis, MO). Sections were then immersed in fixative and placed at -20°C prior to staining.

Neurite and Nuclear Staining—One set of tissue sections were double stained with lipophilic dye “DiI” (1,1'-Dioctadecyl-3,3,3',3'-tetra-methylindocarbocyanine) and nuclear stain (Hoescht-33342). The staining protocol is described elsewhere (Budde and Frank, 2012; Khan et al., 2015). Briefly, sections were dehydrated with graded concentrations of ethanol and then stained with DiI (0.25 mg/ml) in absolute ethanol for approximately 1 minute. The stained sections were then rinsed with absolute ethanol to remove excess dye and then rehydrated by reversing the order of the graded ethanol concentrations. After rehydration, sections were stained with nuclear dye (Hoechst 10 μl /ml) for 10 minutes and subsequently washed with PBS three times. Sections were mounted on Superfrost+ glass slides with fluorescence mounting medium (Dako, Glostrup, Denmark).

Astrocyte immunostaining—One set of tissue slices underwent immunostaining with the astrocyte marker *ALDH1L1* (AbCam, Cambridge, UK). Prior to staining, sections were rinsed with 1X tris buffered saline (TBS). Endogenous peroxidase activity was quenched with a cocktail of TBS, methanol and H_2O_2 (3%) for 15 minutes. Tissue sections were subjected to heat mediated antigen retrieval with target retrieval solution buffer (Dako, Denmark, S1699) at 80°C for 30 min. Thereafter, each section was rinsed three times with TBS (pH 7.4) and incubated with the appropriate blocking buffer for 30 minutes before applying the primary antibody. The sections were stained with *ALDH1L1* (antibody, 1:500, Abcam) overnight at 4°C and subsequently with diluted (1:200) horseradish-peroxidase (HRP) coated secondary antibody (Dako, Glostrup, Denmark) in a TB buffer containing 1% bovine serum albumin (BSA). Antibodies were detected using the HRP complex, and labeling was revealed after incubating the sections in 3,3'-diaminobenzidine (DAB) peroxidase solution (31.5 μl DAB, 1 μl H_2O_2 in 1.6 ml 0.01 M TBS, pH 7.2) for 5 min and the subsequent washing and counterstaining with toluidine blue. Finally, tissue sections were dehydrated in absolute ethanol and subsequently treated with xylene before mounting with permanent mounting medium on Superfrost+ glass slides.

Confocal Microscopy

Image stacks in 3D were obtained with a Zeiss LSM 700 confocal microscope equipped with a 63x/1.20 W Corr water immersion objective using an appropriate filter. The excitation wavelengths for image acquisition from DiI and Hoechst stains were 549 and 480 nanometer respectively. Acquisition of 3D image stacks was performed using Zen2011 Image processing software (Carl Zeiss). Images were imported into Fiji J and converted to ‘tif’ format for further analysis (Schindelin et al., 2012). All images were subjected to similar brightness and contrast adjustment.

Light Microscopy

Immunohistological sections were imaged with a Leica Microscope (Leica DM 6000). Whole tissue section montages were acquired with a 4X objective lens (Figure 3a), and high resolution images were acquired with a 63x oil objective lens (Figure 3b) and 3D image stacks were obtained on confocal microscope (Figure 3c). Systematically sampled fields of views (FOVs) of each section were taken within the Am region of the brain. Images were imported in 'tif' format for further analysis in Matlab (The Mathworks, Natick, MA).

Neurite and nuclear Image analysis

All image analysis was done automatically and with the same settings on all 3D image stacks, in order to ensure objectivity. DiI stained images were used to evaluate an approximate neurite volume fraction, and Hoechst-stained images to estimate approximate nuclear volume fraction (Figure 4a-c and 4d-f, respectively), using the following procedure. DiI stained image stacks were first corrected for depth dependent image intensity variation using a built-in functionality in ImageJ (Schindelin et al., 2012), and image contrast enhancement was applied by contrast-limited adaptive histogram equalization (CLAHE) in Matlab (Figure 4b). Contrast enhanced images were then thresholded into binary images, where pixels equal to or greater than 50% maximum image intensity were set to a value of 1 and others were set to a value of zero. To identify only plausible neurite structures in the resulting image, an area opening operation to remove objects (connected neighborhood) smaller than 40 pixels (~4 μm), considered unlikely to belong to neurites. Nuclear images were thresholded into binary images and the image opening operation was followed with a square (2, 2) structure element created by using the 'strel' function. Holes within the nuclei were then filled using the 'imfill' function. Background pixels were removed using an area opening operation (Figure 4e, 4f). Binary images with morphological structures were visually compared with contrast enhanced images to confirm successful delineation of neurites and nuclei. Finally, the number of foreground pixels in the binary image was counted and normalized to approximate neurite and nuclear volume fractions (Figure 4c, 4f).

Astrocyte Image analysis

All image analysis was done automatically and with the same settings on all images. All immunofluorescent images imported as 'tif' images in Matlab (Figure 4g) were first separated into separate 'rgb' channels after which the blue channel was nulled. The resulting rgb image intensity was then adjusted to enhance contrast and converted into L^*a^*b color space (Hunter, 1948) to scale the luminosity of each image with maximum luminosity. The images were subsequently reconverted into 'rgb' format, and then red and green channels were separately adjusted with contrast-limited adaptive histogram equalization to enhance the contrast for images. Contrast enhanced red and green channel images and blue channel with zero values were again combined in rgb format (Figure 4h). Finally, the contrast enhanced images were thresholded as earlier to binary images to count the pixels within astrocyte cells as an approximate measure of astrocyte volume fraction (Figure 4i).

Statistical analyses

In order to test for significant differences between groups, MRI data and histological data were separately fit in Matlab to (categorical) linear mixed effect models with animals as random effects (i.e. allowing for inter subject variability) and groups (controls/ anhedonic/ resilient) as fixed effects. Significance of group effects using a significance level of 0.05 was assessed with an F-test, where the degrees of freedom were computed using the Satterthwaite approximation (Satterthwaite, 1946): if significant, pairwise tests (3 tests) were performed without correction for multiple comparisons. Confidence intervals (95%) were generated as output as well to provide an estimate of fixed effect size and variability (Cumming, 2013). When applicable, graphs report confidence intervals and estimated means.

RESULTS

Visual inspection of anatomical images of the brains did not indicate any gross changes in any of the brain regions. Figure 2 shows representative maps of MR based neurite density, D_{eff} , D_L , MD, FA, MKT, MK and corresponding T2 weighted image (T2) from control, anhedonic and resilient groups. It is seen that MD, D_{eff} and D_L does not show contrast between gray and white matter regions. MKT and MK are measures of non-Gaussianity of water diffusion in tissue and both show similar contrast in kurtosis maps; particularly, white matter possesses higher kurtosis values than gray matter regions.

Evaluation of biophysical model stability

In order to examine the fitting stability of the biophysical model used in this study, an additional analysis was performed. For this purpose the fit procedure was analysed using 50 randomly chosen voxels and 1000 randomized initial values. Since the picture is qualitatively consistent for clarity reasons Figure 5 shows the partial data of changes in 4 of the estimated parameters based on the signal from 10 randomly chosen voxels taken from one of the scanned brains, for 50 randomized initial values. All of the model parameters in all the analysed voxels are strongly concentrated for the majority of the initial values. The values of the estimates reported in Figure 5 (shown in red in the plot) generally coincide with the clusters (i.e. the stable estimates). Our analysis also showed that the small amount of dispersion around the clusters affects the fit due to voxels with partial volume and low SNR. These outliers correspond to higher error values, than the clustered parameters. Therefore, unlike human brain in-vivo (Jelescu et al., 2016), there is no major degeneracy in the estimation of the parameters in fixed rat brain tissue, meaning that the model parameters are very stable.

MR based Neurite density

Figure 6a shows the mean values of MR based neurite density parameter (ν) for each ROI along with 95% confidence intervals for each group. The neurite density parameter was significantly different between groups only in the Am region of the brain, where a significant higher value was found in the anhedonic group ($p < 0.01$) as well as in the resilient group ($p < 0.01$) compared to controls, however no significant difference was observed between anhedonic and resilient groups (Figure 6a). Similar higher values were also

observed in Pfc in both stressed groups, but the broader confidence intervals here precluded the effect from reaching significance.

Mean of the Kurtosis Tensor (MKT) and Mean Kurtosis (MK)

In Figure 6b and 6c, we show mean values and confidence intervals for the MKT and MK respectively. Similar to MR based neurite density, MKT was significantly different in the Am of anhedonic ($p < 0.01$) and resilient group ($p < 0.01$) (Figure 6b) compared to controls, but no other regions were significantly different between groups. The graph also shows a modestly higher MKT parameter in Pfc, but again the wider confidence intervals prevented the effect from reaching the level of significance. Despite narrower confidence intervals, Hp and Cp were not significantly affected by CMS. With the Hp as the only exception, the qualitative behavior of MK is very similar to MKT, albeit with generally slightly lower values. Nevertheless, no statistically significant difference between groups could be detected for MK.

Mean Diffusivity (MD)

There were no significant variations in the MD parameter except in the Am region (Figure 6d). The Am shows significantly reduced MD in the anhedonic ($p < 0.05$) as well as in the resilient groups ($p < 0.05$). The confidence interval of MD was also notably wider in Pfc than other brain regions.

Extracellular Diffusivity (D_{eff})

There were significantly lower D_{eff} in Am as well as in Hp and Cp (Figure 6e). The significantly lower D_{eff} in Am ($p < 0.05$) and Hp ($p < 0.05$) were observed both in anhedonic and resilient groups, while in Cp, a significantly lower D_{eff} ($p < 0.01$) was observed only in the resilient group, compared to control. Pfc also showed an apparent decrease, however due to the wider confidence interval for D_{eff} in this region, this difference was not statistically significant.

Intra neurite diffusivity (D_L)

D_L was significantly smaller in amygdala of both anhedonic and resilient groups ($p < 0.01$) compared to controls. Similar to other parameters, D_L also showed wider confidence intervals in Pfc, than in Hp and Cp. No other ROIs showed significant alterations in D_L .

Fractional anisotropy (FA)

FA in Am is higher than in the other gray matter regions of the brain, which may be due to the notable FA differences in sub regions of the Am (Kulkarni et al., 2015). Contrary to the other parameters, FA shows narrow confidence intervals in each region of the brain in all three groups, yet no statistically significant differences were found (Figure 6e).

Histology

For purposes of corroborating the MRI findings, histological analyses of the amygdala were performed. The contrast enhanced images stained with DiI from a region consistently identifiable in sections obtained from each animal, residing within the lateral amygdala,

were analyzed in control, anhedonic and resilient animal brains. Increased neurite density was observed in both stressed groups relative to control (Figure 7). The quantitative graph of neurite density estimated from DiI shows significantly higher density in the anhedonic ($p < 0.01$) and the resilient groups ($p < 0.05$) in comparison to the control group (Figure 8), however no significant difference was observed between anhedonic and resilient groups. In order to ensure that a representative region of the Am was sampled in the histological analysis, a secondary analysis was performed on the single MRI voxel that was manually identified to be closest to the analyzed region of the histological section. Although group differences in the single-voxel analysis did not reach statistical significance, presumably due to the low signal-to-noise ratio attainable with a single-voxel analysis, trends for the mean neurite densities for the three groups resembled those of the Am in general, with anhedonic and resilient groups being larger than for controls (data not shown). No significant changes were observed in nuclear density, although a very slight reduction was observed in both stressed groups (Figure 8). Broader confidence intervals were apparent in both CMS groups compared to control for neurite and nuclear density.

There were no significant alterations in astrocyte density among the groups, but a modest non-significant decrease of astrocyte density was observed in anhedonic and resilient groups in comparison to controls (Figure 8). In all cases, the CMS groups appear more similar to each other than to the controls.

DISCUSSION

The present study was undertaken to explore the d-MRI based microstructural changes in stress sensitive regions of anhedonic and resilient rat brains following eight weeks of CMS exposure. The d-MRI based microstructural modifications were further validated with quantitative histology. The CMS model has good, predictive, construct and face validity as a preclinical model of depression (Wiborg, 2013; Willner, 1997, 2005). The CMS model has demonstrated subtle cellular and morphological alterations, however, more notable microstructural alterations were reported in Hp, Pfc and Am (Cohen et al., 2014; Henckens et al., 2015; Jayatissa et al., 2010; Mitra et al., 2005). Traditional neuroimaging modalities have not previously been able to capture these subtle changes. However, recent advancement in biophysical modeling of d-MRI data have made it feasible to estimate specific subcellular microstructures, such as MR based neurite density, as well as other microstructural biomarkers, non-invasively (Fieremans et al., 2011; Jespersen et al., 2010; Jespersen et al., 2007; Novikov et al., 2014). Such novel metrics have huge potential clinical significance in early disease diagnosis and in medical management. The present study utilized MKT, MK, MD, D_{eff} , D_L , FA, and MR based neurite density modeled by volume fraction of the cylindrical component of the diffusion signal (Jespersen et al., 2010; Jespersen et al., 2007). MKT and MK both represent non-Gaussianity of water diffusion in tissue, but in an analytically different manner (Hansen et al., 2013; Hansen et al., 2014). We found significant differences in MR based neurite density, MKT, MD, D_{eff} and D_L in the Am of anhedonic and resilient rat brains. This was supported by quantitative histology, where we found a significant increase in DiI staining based neurite density and non-significant decreases in astrocyte and nuclear staining. Only MR based neurite density changes were supported with histology, since a direct validation of diffusion/kurtosis imaging parameters

through microscopy is not possible due to the limited availability of diffusion sensitive optical microscopy techniques, especially using reporter molecules comparable in size to water. D_{eff} was reduced in Hp in both the stressed groups while Cp showed significantly reduced D_{eff} only in resilient group in comparison to controls. The significant alterations in diffusivity parameters of Hp and Cp, but non-significant changes in MR based neurite density in the corresponding ROIs, indicates caveats against fixing the diffusivity to estimate the neurite density parameter (Zhang et al., 2012).

The MR based neurite density was lowest in the control group, followed by the anhedonic group, and largest in the resilient group, although levels in the two latter groups were not significantly different. A very similar qualitative behavior was found for the MKT, and similar behavior in MKT and MR based neurite density was also observed in all other ROIs. One might anticipate such a correspondence, if e.g. the extracellular space becomes more non-Gaussian with an increased density of neurites, but the degree of similarity is striking. These results suggest that the MKT is largely driven by neurite density, at least in the Am of the current model. MK was also quite similar to MKT, an observation also made in previous studies (Glenn et al., 2015; Hansen et al., 2013). On the other hand, MD decreased significantly in the stressed groups, which again is consistent with increased density of neurites and a more tortuous extracellular space. The significant decrease in D_{eff} also indicates the increased tortuosity of extracellular space of Am as well as Hp and Cp. The apparent increase in MR based neurite density in Hp and Cp may be a factor in the significant decrease of D_{eff} in Hp and Cp. Although the diffusivity parameters (MD, D_{eff} and D_L) also revealed an effect of the stress paradigm, these parameters are difficult to interpret in terms of a specific cellular-level event and could in principle be ascribed to multiple sources. This is in contrast to neurite density which identifies the biological underpinnings of the diffusivity changes. Indeed, the results from histology corroborated these MRI findings. In particular, quantification of neurite density based on DiI staining confirmed the significantly higher neurite density in the Am, although histological neurite density percentage may be numerically underestimated due to under segmentation of DiI stained images. The semi-quantitative measurements of astrocyte density suggested that this occurred at the expense of astrocyte volume fraction, although the differences were non-significant. Nuclear staining density was highly similar between groups, suggesting that processes associated with cell number, such as cell death, in the Am were limited, and that the microstructural changes were mainly due to remodeling of cellular processes. Stereological studies have reported reduced number of glial cells in the Am and Pfc of major depressive disorder and bipolar disorder cases (Bowley et al., 2002; Rajkowska, 2000; Rajkowska et al., 1999). More accurate and specific stereological studies in stress sensitive regions of the brain are required to establish neuronal and glial cell plasticity in depression.

In the stressed state, the Am activates stress pathways in the hypothalamus and the brainstem, evoking release of noradrenalin and dopamine which in turn impairs Pfc function but increases Am activity (Arnsten, 2009). Hyperactivity in the Am strengthens memories of emotionally significant experiences related to severe or chronic stress (Mitra et al., 2005; Roozendaal et al., 2009). A few preclinical studies on stress and depression have reported neuronal remodeling as well as increased dendritic length and enhanced spinogenesis in Am using neuronal tracing techniques (Henckens et al., 2015; Mitra et al., 2005; Vyas et al.,

2003; Vyas et al., 2006; Vyas et al., 2002). For example, Vyas et al 2002 demonstrated stress-induced dendritic atrophy in Hp but hypertrophy in pyramidal neurons of basolateral Am in a rat model of unpredictable chronic stress. They further emphasized that the observed Am hypertrophy in response to chronic stress persists for a number of weeks after the termination of the stressful stimuli. The underlying mechanisms behind this differential phenotype after CMS exposure in Hp and Am might be due to differential expression of various neurotrophic factors, such as brain-derived neurotrophic factor (BDNF) (Boyle, 2013; Egeland et al., 2015; Krishnan and Nestler, 2008). The increase in the MR based neurite density parameter found here is corroborated by these previous findings, but conversely we found no significant alterations in MR based neurite density parameters in Hp, Pfc and Cp regions of the brain. This may be due to variability, or contrasting effects previously reported among sub regions of Hp and Pfc (Arnsten, 2009; Cerqueira et al., 2007; Cohen et al., 2014; Henckens et al., 2015; Radley et al., 2006), or the effect being too small to be significant in the MRI experiments. Future investigations focusing on the sub regions of Am, Pfc and Hp with advanced neuroimaging strategies and histology might be able to elucidate this.

Radley et al. (2004) demonstrated reductions in apical dendrite lengths after chronic restraint stress. This is in contrast to y Palacios et al. (2014) who reported significant increases in radial diffusivity in Am and no significant alteration in MD, while a significant decrease in MD was observed in the present study. This contrasting effect might be due to differences between the in-vivo and ex-vivo experimental conditions, and are also apparent with the notable difference in MD values in both setups. In addition to the in-vivo and ex-vivo experimental conditions, different diffusion protocols as well as different voxel sizes cause the results to not be directly comparable. Another in-vivo study on unpredictable CMS rat brain by y Palacios et al. (y Palacios et al., 2011) demonstrated significant reductions in MK and radial kurtosis in anhedonic and resilient animals, with unaffected kurtosis anisotropy, MD and FA. Although Hp is also considered sensitive to stress and a decreased volume is one of the most consistent clinical findings in depressed patients (Kempton et al., 2011), the vast heterogeneity in symptoms and etiology of depression might be the reason why we have only observed significant reduction in D_{eff} in Hp. The CMS model also causes functional impairment and ^1H magnetic resonance spectroscopy based metabolic changes can add substantial information for diagnosis and therapy (Hasler and Northoff, 2011), however, microstructural changes can be considered as relatively stable biomarker in disease diagnoses and therapeutic interventions. A longitudinal study of functional and microstructural alterations due to CMS would provide a better understanding of adaptive and maladaptive response in different regions of the brain. In addition pathophysiology based neuroimaging measures could improve the phenotypic definition of chronic stress.

CONCLUSION

The present study shows that neurite density, as measured by d-MRI, is larger in Am of CMS brains, which explicitly supports previous reports of microscopy based dendritic hypertrophy in Am after chronic stress. MKT, MD, D_{eff} and D_L also showed significant changes, in Am as well as in Hp and Cp. However, it was not possible to directly validate these findings with microscopy in this study. Quantitative validation of d-MRI based

parameters establishes a better understanding of microstructural modification in terms of the d-MRI signal. These d-MRI based parameters may potentially be used in clinical contexts to explore microstructural changes in chronic stress and/or major depressive disorder.

Acknowledgement

Lundbeck Foundation grants R83–A7548 and Simon Fougner Hartmanns Familie fond. AC and BH acknowledge supported from NIH 1R01EB012874-01. The authors wish to thank Arnela Mehmedbasic (Department of Biomedicine, Aarhus University) for help with image acquisition on confocal microscope. Lippert's Foundation and Korning's Foundation for financial support. The 9.4T lab was made possible by funding from the Danish Research Council's Infrastructure program, the Velux Foundations, and the Department of Clinical Medicine, AU. Centre for Stochastic Geometry and Advanced Bioimaging is supported by Villum Foundation.

References

- American Psychiatric Association. Diagnostic and statistical manual of mental disorders. 5th ed. Washington, DC: 2013.
- Anacker C, Scholz J, O'Donnell KJ, Allemang-Grand R, Diorio J, Bagot RC, Nestler E, Hen R, Lerch JP, Meaney MJ. Neuroanatomical differences associated with stress susceptibility and resilience. *Biological psychiatry*. 2015
- Arnsten AF. Stress signalling pathways that impair prefrontal cortex structure and function. *Nature Reviews Neuroscience*. 2009; 10:410–422. [PubMed: 19455173]
- Basser PJ. Inferring microstructural features and the physiological state of tissues from diffusion-weighted images. *NMR in Biomedicine*. 1995; 8:333–344. [PubMed: 8739270]
- Basser PJ. New Histological and Physiological Stains Derived from Diffusion-Tensor MR Images. *Annals of the New York Academy of Sciences*. 1997; 820:123–138. [PubMed: 9237452]
- Bourgin J, Cachia A, Boumezbear F, Djemaï B, Bottlaender M, Duchesnay E, Mériaux S, Jay T. Hyper-responsivity to stress in rats is associated with a large increase in amygdala volume. A 7T MRI study. *European Neuropsychopharmacology*. 2015; 25:828–835. [PubMed: 25823695]
- Bowley MP, Drevets WC, Öngür D, Price JL. Low glial numbers in the amygdala in major depressive disorder. *Biological psychiatry*. 2002; 52:404–412. [PubMed: 12242056]
- Boyle LM. A neuroplasticity hypothesis of chronic stress in the basolateral amygdala. *The Yale journal of biology and medicine*. 2013; 86:117. [PubMed: 23766733]
- Budde MD, Frank JA. Examining brain microstructure using structure tensor analysis of histological sections. *NeuroImage*. 2012; 63:1–10. [PubMed: 22759994]
- Cerqueira JJ, Taipa R, Uylings HB, Almeida OF, Sousa N. Specific configuration of dendritic degeneration in pyramidal neurons of the medial prefrontal cortex induced by differing corticosteroid regimens. *Cerebral Cortex*. 2007; 17:1998–2006. [PubMed: 17082516]
- Christoffel DJ, Golden SA, Russo SJ. Structural and synaptic plasticity in stress-related disorders. *Reviews in the neurosciences*. 2011; 22:535–549. [PubMed: 21967517]
- Cohen H, Kozlovsky N, Matar MA, Zohar J, Kaplan Z. Distinctive hippocampal and amygdalar cytoarchitectural changes underlie specific patterns of behavioral disruption following stress exposure in an animal model of PTSD. *European Neuropsychopharmacology*. 2014; 24:1925–1944. [PubMed: 25451698]
- Cumming G. The new statistics why and how. *Psychological science*. 2013 0956797613504966.
- De Kloet ER, Joëls M, Holsboer F. Stress and the brain: from adaptation to disease. *Nature Reviews Neuroscience*. 2005; 6:463–475. [PubMed: 15891777]
- Egeland M, Zunszain PA, Pariante CM. Molecular mechanisms in the regulation of adult neurogenesis during stress. *Nature Reviews Neuroscience*. 2015; 16:189–200. [PubMed: 25790864]
- Enzinger C, Barkhof F, Ciccarelli O, Filippi M, Kappos L, Rocca MA, Ropele S, Rovira À, Schneider T, de Stefano N. Nonconventional MRI and microstructural cerebral changes in multiple sclerosis. *Nature Reviews Neurology*. 2015; 11:676–686. [PubMed: 26526531]

- Ferrari AJ, Charlson FJ, Norman RE, Patten SB, Freedman G, Murray CJ, Vos T, Whiteford HA. Burden of depressive disorders by country, sex, age, and year: findings from the global burden of disease study 2010. *PLoS one*. 2013:e1001547.
- Fieremans E, Jensen JH, Helpert JA. White matter characterization with diffusional kurtosis imaging. *NeuroImage*. 2011; 58:177–188. [PubMed: 21699989]
- George, P.; Charles, W. Qingchuan Zhuge translate. People's Medical Publishing House; Beijing, China: 1998. The rat brain in stereotaxic coordinates.; p. 322007
- Glenn GR, Helpert JA, Tabesh A, Jensen JH. Quantitative assessment of diffusional kurtosis anisotropy. *NMR in Biomedicine*. 2015; 28:448–459. [PubMed: 25728763]
- Hansen B, Jespersen SN. Kurtosis fractional anisotropy, its contrast and estimation by proxy. *Sci Rep*. 2016; 6:23999. [PubMed: 27041679]
- Hansen B, Lund TE, Sangill R, Jespersen SN. Experimentally and computationally fast method for estimation of a mean kurtosis. *Magn Reson Med*. 2013; 69:1754–1760. [PubMed: 23589312]
- Hansen B, Lund TE, Sangill R, Jespersen SN. Magnetic Resonance in Medicine. 2014; 71:2250–2250. Erratum: Hansen, Lund, Sangill, and Jespersen. Experimentally and Computationally Fast Method for Estimation of a Mean Kurtosis. *Magnetic Resonance in Medicine* 69: 1754–1760 (2013).
- Hasler G, Northoff G. Discovering imaging endophenotypes for major depression. *Molecular psychiatry*. 2011; 16:604–619. [PubMed: 21602829]
- Henckens MJ, van der Marel K, van der Toorn A, Pillai AG, Fernández G, Dijkhuizen RM, Joëls M. Stress-induced alterations in large-scale functional networks of the rodent brain. *NeuroImage*. 2015; 105:312–322. [PubMed: 25462693]
- Hori M, Fukunaga I, Masutani Y, Taoka T, Kamagata K, Suzuki Y, Aoki S. Visualizing non-Gaussian diffusion: clinical application of q-space imaging and diffusional kurtosis imaging of the brain and spine. *Magnetic Resonance in Medical Sciences*. 2012; 11:221–233. [PubMed: 23269009]
- Hunter RS. Accuracy, precision, and stability of new photoelectric color-difference meter. *Journal of the Optical Society of America*. 1948; 38:1094–1094.
- Jayatissa MN, Bisgaard C, Tingström A, Papp M, Wiborg O. Hippocampal cytochrome oxidase correlates to escitalopram-mediated recovery in a chronic mild stress rat model of depression. *Neuropsychopharmacology*. 2006; 31:2395–2404. [PubMed: 16482085]
- Jayatissa MN, Henningsen K, Nikolajsen G, West MJ, Wiborg O. A reduced number of hippocampal granule cells does not associate with an anhedonia-like phenotype in a rat chronic mild stress model of depression. *Stress*. 2010; 13:95–105. [PubMed: 19929309]
- Jelencu IO, Veraart J, Fieremans E, Novikov DS. Degeneracy in model parameter estimation for multi-compartmental diffusion in neuronal tissue. *NMR in Biomedicine*. 2016; 29:33–47. [PubMed: 26615981]
- Jensen JH, Helpert JA. MRI quantification of non-Gaussian water diffusion by kurtosis analysis. *NMR in Biomedicine*. 2010; 23:698–710. [PubMed: 20632416]
- Jensen JH, Helpert JA, Ramani A, Lu H, Kaczynski K. Diffusional kurtosis imaging: The quantification of non-gaussian water diffusion by means of magnetic resonance imaging. *Magnetic Resonance in Medicine*. 2005; 53:1432–1440. [PubMed: 15906300]
- Jespersen S, Bjarkam C, Nyengaard J, Chakravarty M, Hansen B, Vosegaard T, Ostergaard L, Yablonskiy D. Neurite density from magnetic resonance diffusion measurements at ultrahigh field: comparison with light microscopy and electron microscopy. *NeuroImage*. 2010; 49:205–216. [PubMed: 19732836]
- Jespersen SN, Kroenke CD, Ostergaard L, Ackerman JJ, Yablonskiy DA. Modeling dendrite density from magnetic resonance diffusion measurements. *NeuroImage*. 2007; 34:1473–1486. [PubMed: 17188901]
- Kalisch R, Schubert M, Jacob W, Keßler MS, Hemauer R, Wigger A, Landgraf R, Auer DP. Anxiety and hippocampus volume in the rat. *Neuropsychopharmacology*. 2006; 31:925–932. [PubMed: 16192979]
- Kellner E, Dhital B, Kiselev VG, Reiser M. Gibbs-ringing artifact removal based on local subvoxel-shifts. *Magnetic Resonance in Medicine*. 2015

- Kempton MJ, Salvador Z, Munafò MR, Geddes JR, Simmons A, Frangou S, Williams SC. Structural neuroimaging studies in major depressive disorder: meta-analysis and comparison with bipolar disorder. *Archives of general psychiatry*. 2011; 68:675–690. [PubMed: 21727252]
- Khan AR, Cornea A, Leigland LA, Kohama SG, Jespersen SN, Kroenke CD. 3D structure tensor analysis of light microscopy data for validating diffusion MRI. *NeuroImage*. 2015; 111:192–203. [PubMed: 25665963]
- Krishnan V, Nestler EJ. The molecular neurobiology of depression. *Nature*. 2008; 455:894–902. [PubMed: 18923511]
- Kulkarni P, Kenkel W, Finklestein SP, Barchet TM, Ren J, Davenport M, Shenton ME, Kikinis Z, Nedelman M, Ferris CF. Use of Anisotropy, 3D Segmented Atlas, and Computational Analysis to Identify Gray Matter Subcortical Lesions Common to Concussive Injury from Different Sites on the Cortex. *PLoS one*. 2015:e0125748. [PubMed: 25955025]
- Manji HK, Moore GJ, Rajkowska G, Chen G. Neuroplasticity and cellular resilience in mood disorders. *Molecular psychiatry*. 2000; 5:578–593. [PubMed: 11126389]
- Mathers, C.; Fat, DM.; Boerma, JT. The global burden of disease: 2004 update. World Health Organization; 2008.
- Mitra R, Jadhav S, McEwen BS, Vyas A, Chattarji S. Stress duration modulates the spatiotemporal patterns of spine formation in the basolateral amygdala. *Proceedings of the National Academy of Sciences of the United States of America*. 2005; 102:9371–9376. [PubMed: 15967994]
- Nestler EJ, Barrot M, DiLeone RJ, Eisch AJ, Gold SJ, Monteggia LM. Neurobiology of depression. *Neuron*. 2002; 34:13–25. [PubMed: 11931738]
- Novikov DS, Jensen JH, Helpert JA, Fieremans E. Revealing mesoscopic structural universality with diffusion. *Proceedings of the National Academy of Sciences*. 2014; 111:5088–5093.
- Perrone D, Aelterman J, Pižurica A, Jeurissen B, Philips W, Leemans A. The effect of Gibbs ringing artifacts on measures derived from diffusion MRI. *NeuroImage*. 2015; 120:441–455. [PubMed: 26142273]
- Radley J, Sisti H, Hao J, Rocher AB, McCall T, Hof P, McEwen B, Morrison J. Chronic behavioral stress induces apical dendritic reorganization in pyramidal neurons of the medial prefrontal cortex. *Neuroscience*. 2004; 125:1–6. [PubMed: 15051139]
- Radley JJ, Rocher AB, Miller M, Janssen WG, Liston C, Hof PR, McEwen BS, Morrison JH. Repeated stress induces dendritic spine loss in the rat medial prefrontal cortex. *Cerebral Cortex*. 2006; 16:313–320. [PubMed: 15901656]
- Rajkowska G. Postmortem studies in mood disorders indicate altered numbers of neurons and glial cells. *Biological psychiatry*. 2000; 48:766–777. [PubMed: 11063973]
- Rajkowska G, Miguel-Hidalgo JJ, Wei J, Dilley G, Pittman SD, Meltzer HY, Overholser JC, Roth BL, Stockmeier CA. Morphometric evidence for neuronal and glial prefrontal cell pathology in major depression. *Biological psychiatry*. 1999; 45:1085–1098. [PubMed: 10331101]
- Roosendaal B, McEwen BS, Chattarji S. Stress, memory and the amygdala. *Nature Reviews Neuroscience*. 2009; 10:423–433. [PubMed: 19469026]
- Satterthwaite FE. An approximate distribution of estimates of variance components. *Biometrics bulletin*. 1946:110–114. [PubMed: 20287815]
- Schindelin J, Arganda-Carreras I, Frise E, Kaynig V, Longair M, Pietzsch T, Preibisch S, Rueden C, Saalfeld S, Schmid B. Fiji: an open-source platform for biological-image analysis. *Nature methods*. 2012; 9:676–682. [PubMed: 22743772]
- Stockmeier CA, Mahajan GJ, Konick LC, Overholser JC, Jurjus GJ, Meltzer HY, Uylings HB, Friedman L, Rajkowska G. Cellular changes in the postmortem hippocampus in major depression. *Biological psychiatry*. 2004; 56:640–650. [PubMed: 15522247]
- Tabesh A, Jensen JH, Ardekani BA, Helpert JA. Estimation of tensors and tensor-derived measures in diffusional kurtosis imaging. *Magnetic Resonance in Medicine*. 2011; 65:823–836. [PubMed: 21337412]
- Veraart J, Fieremans E, Jelescu IO, Knoll F, Novikov DS. Gibbs ringing in diffusion MRI. *Magnetic Resonance in Medicine*. 2015

- Veraart J, Van Hecke W, Sijbers J. Constrained maximum likelihood estimation of the diffusion kurtosis tensor using a Rician noise model. *Magnetic Resonance in Medicine*. 2011; 66:678–686. [PubMed: 21416503]
- Vestergaard-Poulsen P, Wegener G, Hansen B, Bjarkam CR, Blackband SJ, Nielsen NC, Jespersen SN. Diffusion-weighted MRI and quantitative biophysical modeling of hippocampal neurite loss in chronic stress. *PloS one*. 2011; 6:e20653. [PubMed: 21747929]
- Vyas A, Bernal S, Chattarji S. Effects of chronic stress on dendritic arborization in the central and extended amygdala. *Brain research*. 2003; 965:290–294. [PubMed: 12591150]
- Vyas A, Jadhav S, Chattarji S. Prolonged behavioral stress enhances synaptic connectivity in the basolateral amygdala. *Neuroscience*. 2006; 143:387–393. [PubMed: 16962717]
- Vyas A, Mitra R, Rao BS, Chattarji S. Chronic stress induces contrasting patterns of dendritic remodeling in hippocampal and amygdaloid neurons. *The Journal of Neuroscience*. 2002; 22:6810–6818. [PubMed: 12151561]
- Wiborg O. Chronic mild stress for modeling anhedonia. *Cell and tissue research*. 2013; 354:155–169. [PubMed: 23801433]
- Willner P. Validity, reliability and utility of the chronic mild stress model of depression: a 10-year review and evaluation. *Psychopharmacology*. 1997; 134:319–329.
- Willner P. Chronic mild stress (CMS) revisited: consistency and behavioural-neurobiological concordance in the effects of CMS. *Neuropsychobiology*. 2005; 52:90–110. [PubMed: 16037678]
- y Palacios RD, Campo A, Henningsen K, Verhoye M, Poot D, Dijkstra J, Van Audekerke J, Benveniste H, Sijbers J, Wiborg O. Magnetic resonance imaging and spectroscopy reveal differential hippocampal changes in anhedonic and resilient subtypes of the chronic mild stress rat model. *Biological psychiatry*. 2011; 70:449–457. [PubMed: 21762877]
- y Palacios RD, Verhoye M, Henningsen K, Wiborg O, Van der Linden A. Diffusion kurtosis imaging and high-resolution MRI demonstrate structural aberrations of caudate putamen and amygdala after chronic mild stress. *PloS one*. 2014;9.
- Zhang H, Schneider T, Wheeler-Kingshott CA, Alexander DC. NODDI: practical in vivo neurite orientation dispersion and density imaging of the human brain. *NeuroImage*. 2012; 61:1000–1016. [PubMed: 22484410]

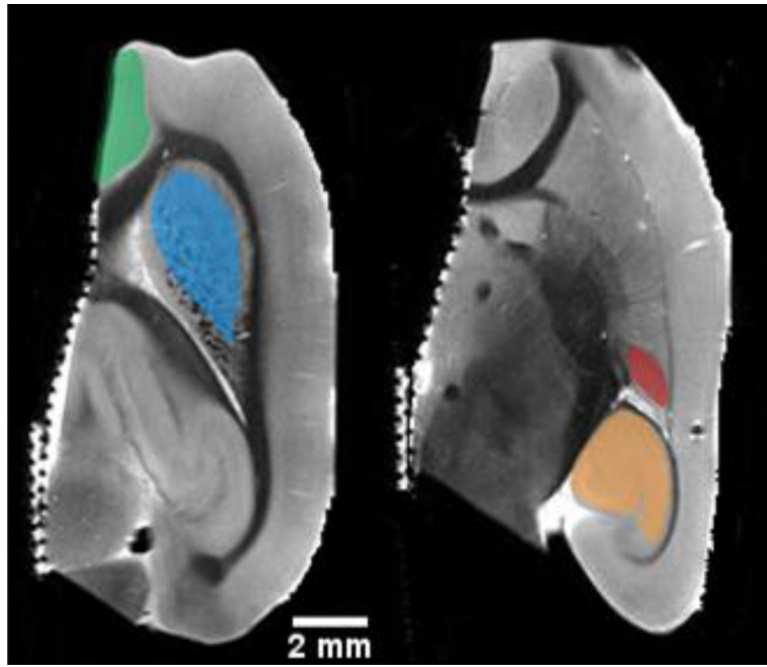


Figure1. T2 weighted image of rat brain hemisphere with ROIs on medial prefrontal cortex (green), caudate putamen (blue), amygdala (brown), and hippocampus (orange).

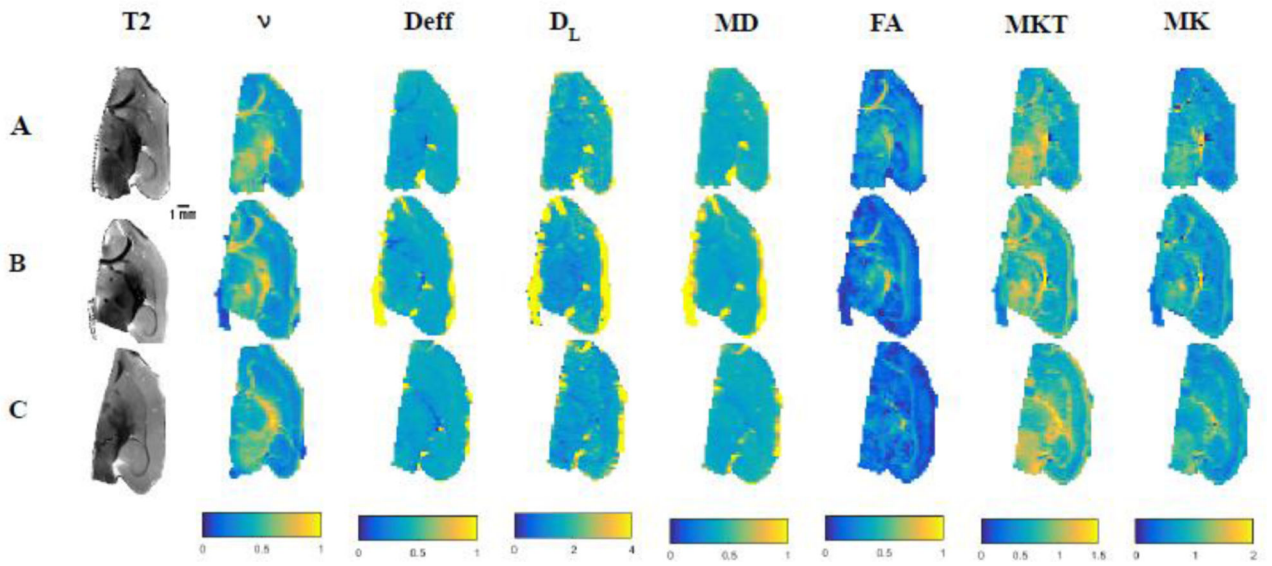


Figure 2. Examples of anatomical T2 weighted image (T2), neurite density (v), D_{eff} , D_L , MD, FA, MKT, and MK, maps from control (A), anhedonic (B) and resilient group(C). Scale bar 1 mm.

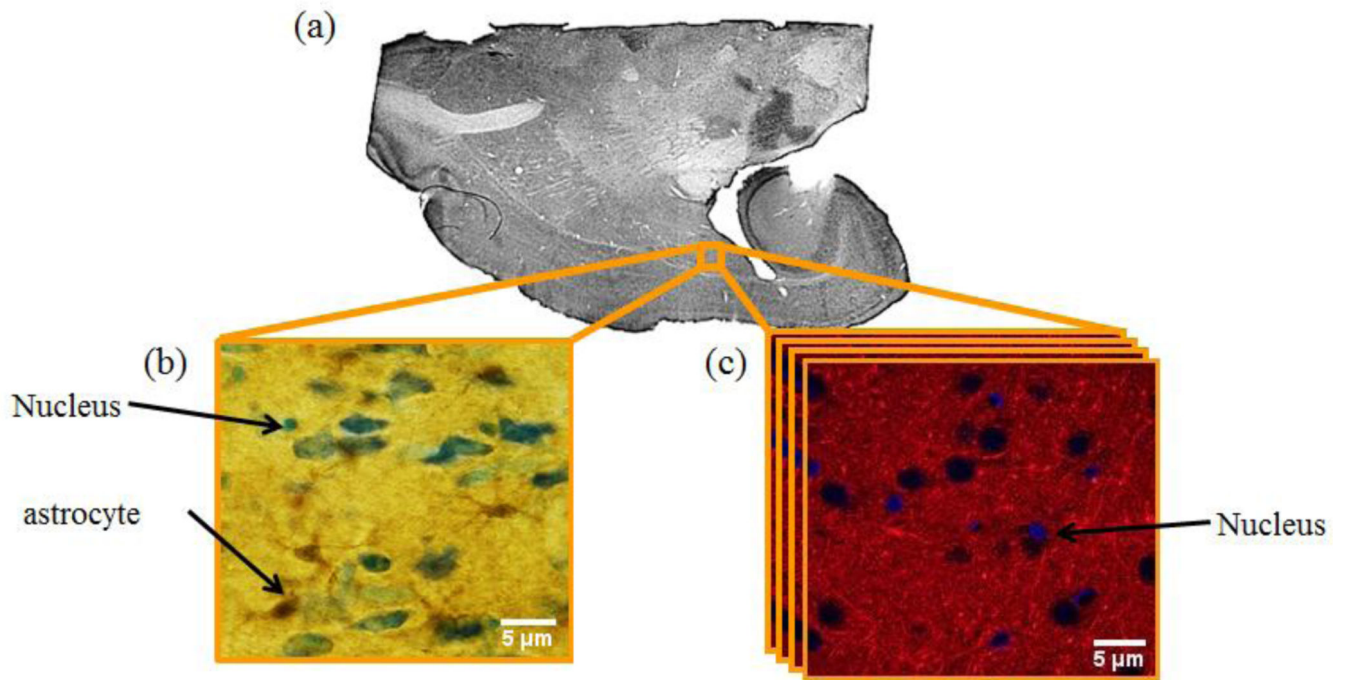


Figure3.

(a) A whole tissue section montage acquired on light microscope with 4X objective. (b) An immuno-stained image with astrocyte marker protein (*ALDH1L1*) counterstained with toluidine blue acquired on light microscope with 63x oil objective and (c) DiI and Hoechst stained 3D image acquired with 63x water objective on confocal microscope.

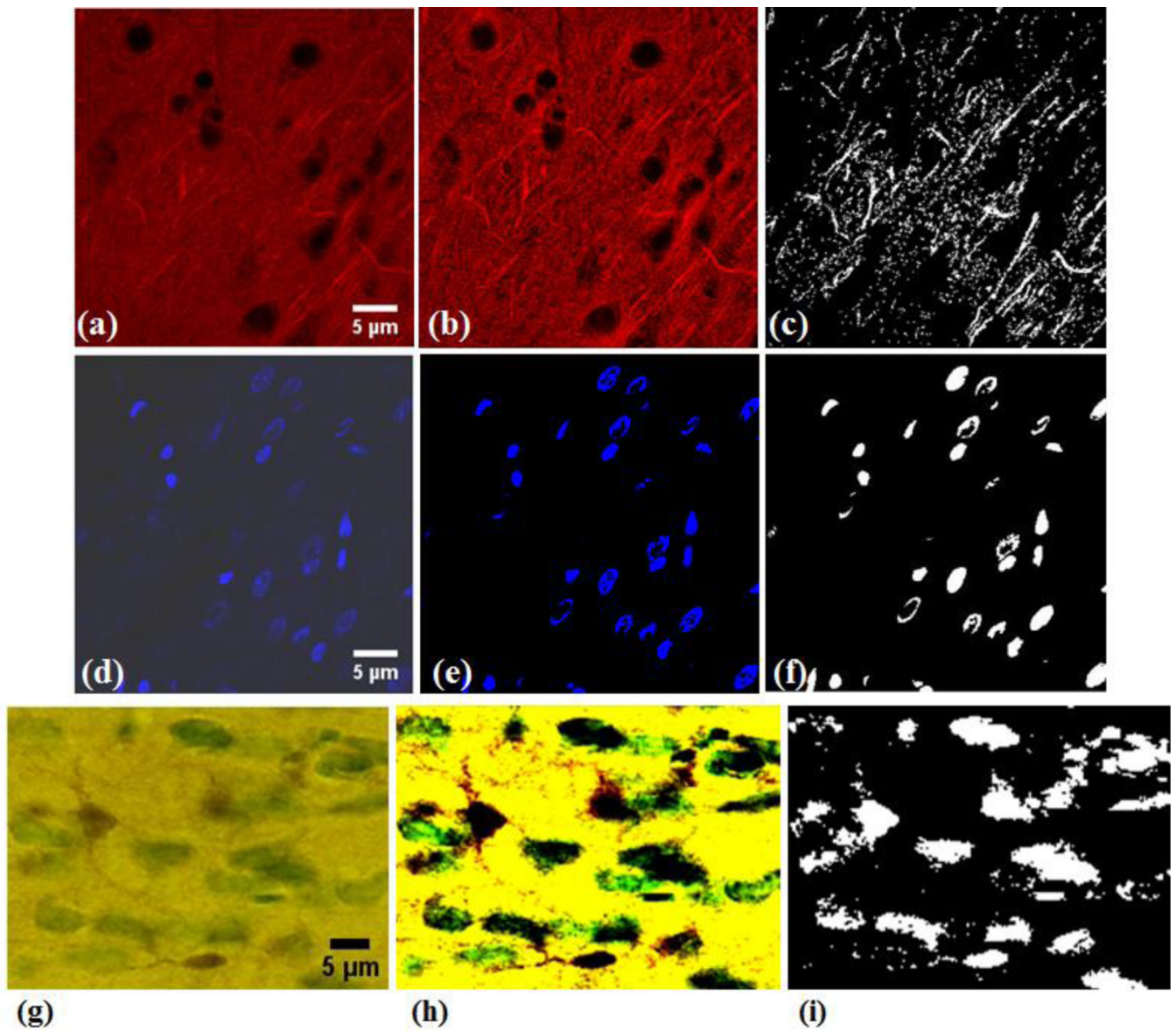


Figure 4.

(a) Original DiI stained Image, (b) Contrast enhanced DiI Image and (c) Binary image reconstructed by morphological operation of contrast enhanced DiI image in Matlab. (d) Original image with nuclear staining, (e) contrast enhanced nuclear image and (f) Binary image reconstructed from contrast enhanced image. (g) Original astrocyte immunohistological image, (h) Contrast enhanced astrocyte image and (i) Binary image reconstructed from contrast enhanced image.

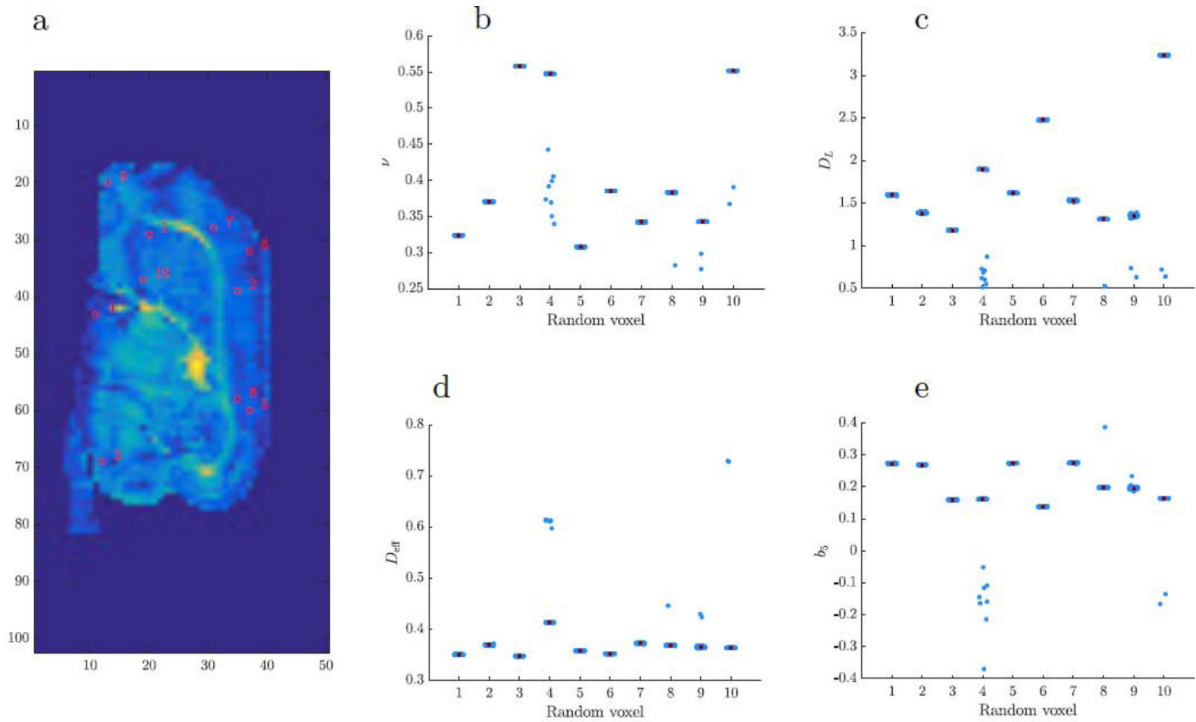
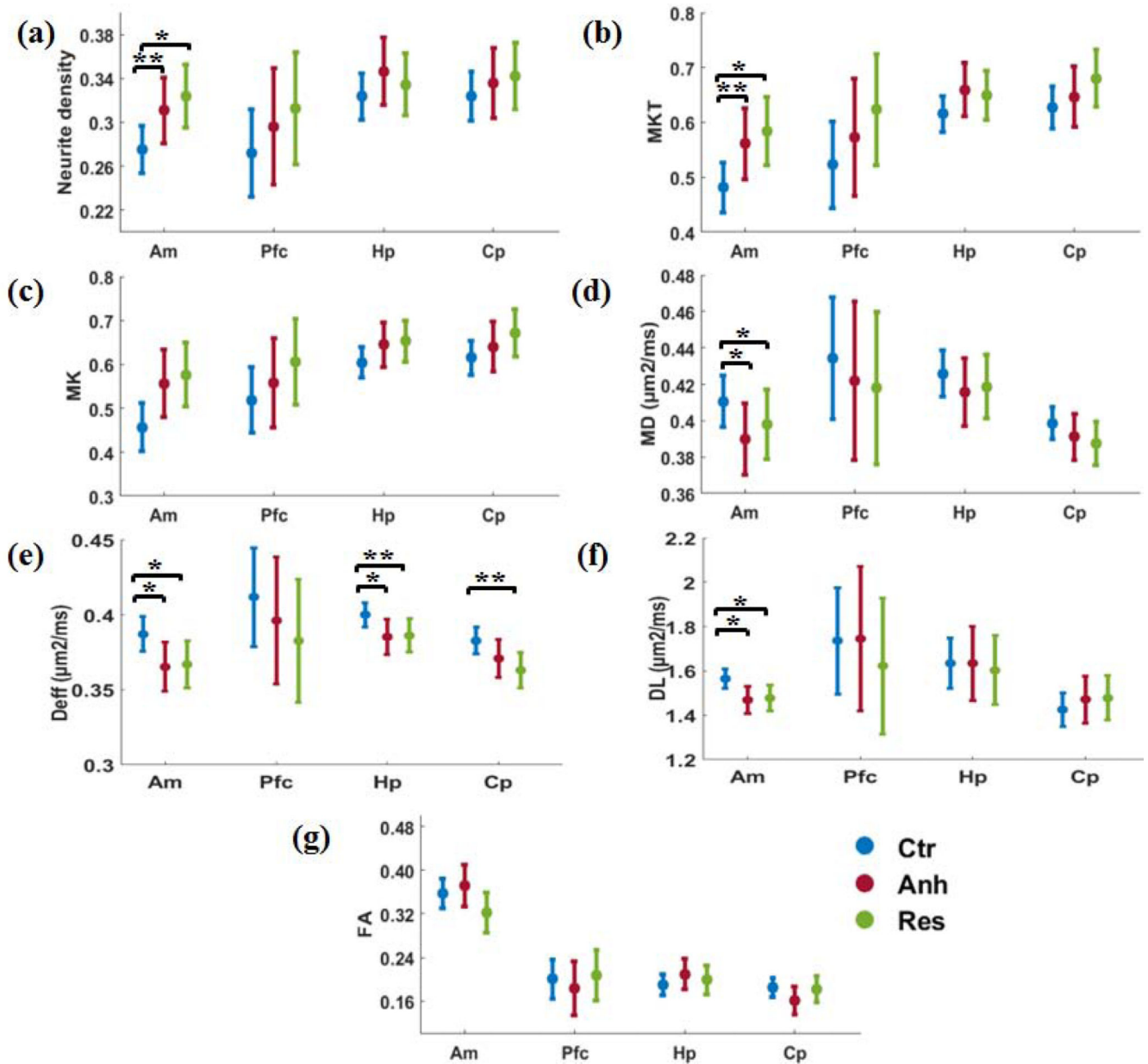


Figure 5.

Verification of the fit stability (biophysical model). (a) The map of the 10 voxels randomly chosen for the evaluation superimposed on the FA map of the brain slice, and variation of various model parameters; (b) neurite density (ν); (c) longitudinal diffusivity in neurites (D_L); (d) diffusivity of the extra-axonal space (D_{eff}); (e) one of the expansion coefficients of the orientation distribution function. Red dots indicate the values that were obtained and used for this study. The goodness of fit (squared error) of points outside of the clusters is significantly poorer (higher squared error) than of the clustered values. For clarity purposes the picture represents only a part of significantly bigger sample of grey matter voxels that were analyzed and only 5% of random initial values. The overall behavior of this small sample is representative and full data is available on demand.

**Figure 6.**

(a) Neurite density (ν), (b) mean kurtosis tensor (MKT), (c) mean kurtosis (MK), (d) mean diffusivity (MD) ($\mu\text{m}^2/\text{ms}$), (e) Extracellular diffusivity (D_{eff}) ($\mu\text{m}^2/\text{ms}$), (f) Intra neurite diffusivity (D_L) ($\mu\text{m}^2/\text{ms}$) and (g) fractional anisotropy (FA) data as mean \pm confidence interval (CI) from Am, Pfc, Hp and Cp regions of the brain from control, anhedonic and resilient group. Linear mixed model regression analysis was performed on Matlab. Significant increase in neurite density and MKT was observed in Am of anhedonic and resilient group (** p < 0.01) in comparison to control while MD, D_{eff} , D_L also shows significant decrease (* p < 0.05) in Am anhedonic and resilient group in comparison to control. D_{eff} also showed significant decrease in Hp in anhedonic group (p < 0.05) and

resilient group ($p < 0.01$) while Cp showed significant decrease in resilient group only ($p < 0.01$) in comparison to control.

Author Manuscript

Author Manuscript

Author Manuscript

Author Manuscript

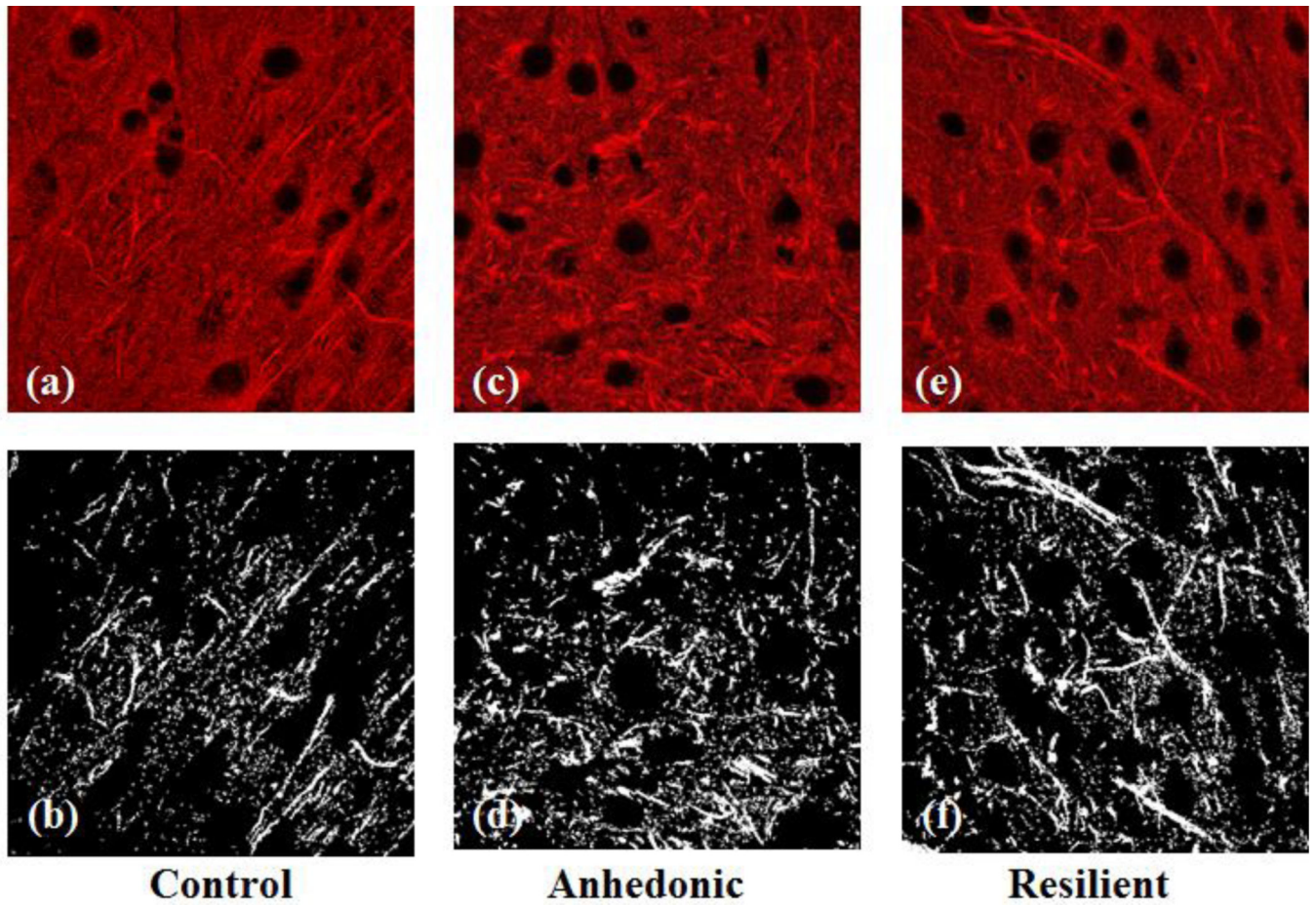


Figure 7.
Contrast enhanced DiI image and corresponding binary image from Am region of brain of control (a), (b), anhedonic (c), (d), and resilient (e), (f) rats.

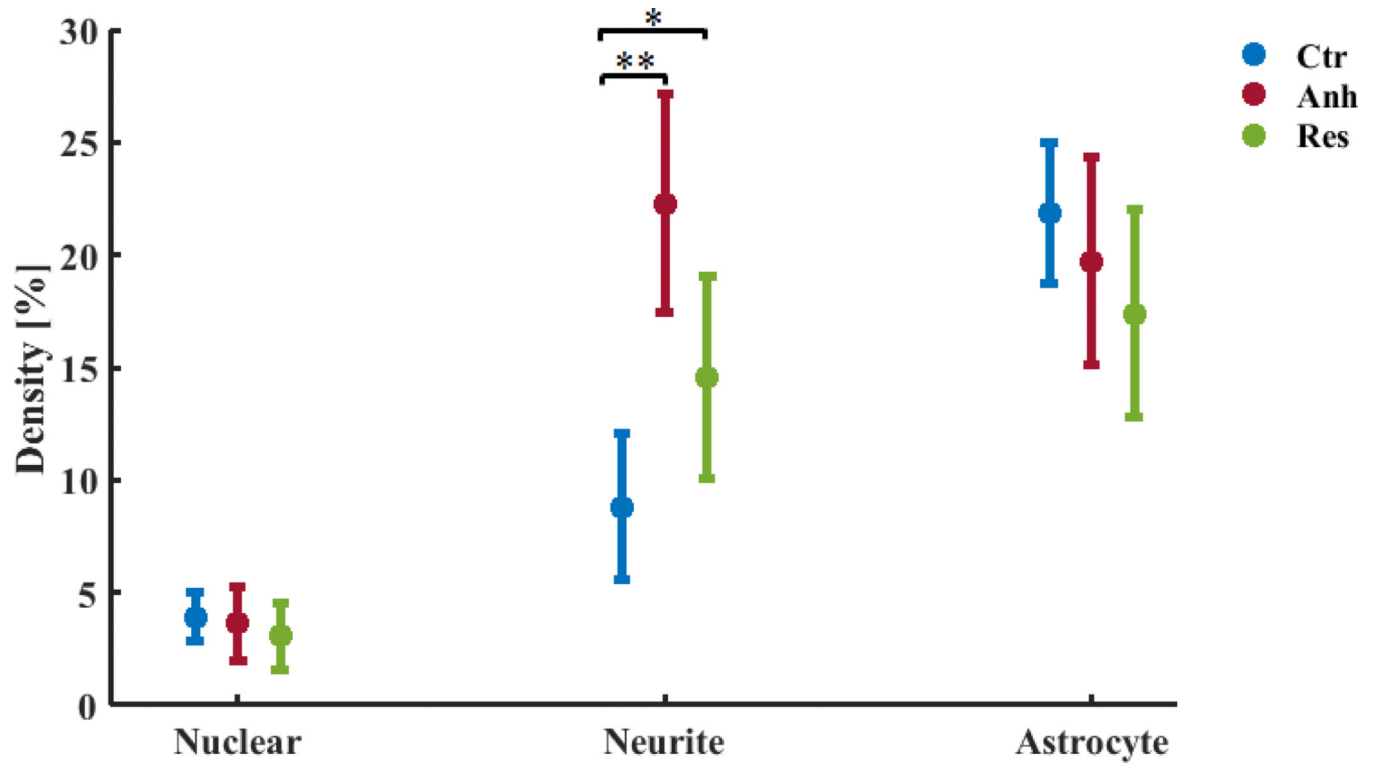


Figure 8. Nuclear, neurite and glial density [%] (mean ± confidence interval) from the amygdala region of the brain. No significant alteration was observed in nuclear density. Neurite density shows significant increase in anhedonic (** $p < 0.01$) and resilient group (* $p < 0.05$) in comparison to control. No significant alteration was observed in astrocyte density [%].